Inorganic Chemistry

pubs.acs.org/IC Article

Cu(I)−I-2,4-diaminopyrimidine Coordination Polymers with Optoelectronic Properties as a Proof of Concept for Solar Cells

Jesus López, Javier González Platas, Ulises Ruymán Rodríguez-Mendoza, José Ignacio Martínez, Salomé Delgado, Ginés Lifante-Pedrola, Eugenio Cantelar, Ricardo Guerrero-Lemus, Cecilio Hernández-Rodríguez, and Pilar Amo-Ochoa*

Cite This: *Inorg. Chem.* 2021, 60, 1208−1219 Read Online

ACCESS | Metrics & More | Article Recommendations | Supporting Information

ABSTRACT: Two coordination polymers with formulas $[CuI(dapym)]_n$ and $[Cu_2I_2(dapym)]_n$ (dapym = 2,4-diaminopyrimidine) have been synthesized in water at room temperature. According to the stoichiometry used, mono (1D) and the two-dimensional (2D) structures can be obtained. Both are made up of Cu_2I_2 double chains. Their high insolubility in the reaction medium also makes it possible to obtain them on a nanometric scale. Their structural flexibility and short Cu−Cu distances provoke interesting optoelectronic properties and respond to physical stimuli such as pressure and temperature, making them interesting for sensor applications. The experimental and theoretical studies allow us to propose different emission mechanisms with different behaviors despite containing the same organic ligand. These behaviors are attributed to their structural differences. The emission spectra versus pressure and temperature suggest competencies between different transitions, founding critical Cu_2I_2 environments, i.e., symmetric in the 1D compound and asymmetric for the 2D one. The intensity in the 2D compound's emission increases with decreasing temperature, and this behavior can be rationalized with a structural constriction that decreases the Cu−Cu and Cu−I distances. However, compound 1D exhibits a contrary behavior that may be related to a change of the organic ligand's molecular configuration. These changes imply that a more significant Π−Π interaction counteracts the contraction in distances and angles when the temperature decreased. Also, the experimental conductivity measurements and theoretical calculations show a semiconductor behavior. The absorption of the 1D compound in UV, its intense emission at room temperature, and the reduction to nanometric size have allowed us to combine it homogeneously with ethyl vinyl acetate (EVA), creating a new composite material. The external quantum efficiency of this material in a Si photovoltaic mini-module has shown that this compound is an active species with application in solar cells since it can move the photons of the incident radiation (UV region) to longer wavelengths.

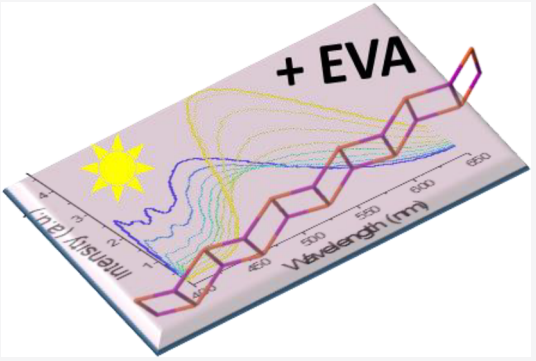

INTRODUCTION

Cu(I)−halogen coordination polymers (CPs) are highly known for their interesting photoluminescent properties.[1−8] Their emission has been studied for decades, and many works have been reported trying to explain their mechanisms.[9−12] Besides this, their low cost (compared with other luminescent coordination polymers, based on gold, silver, or lanthanides),[13] their easy synthesis (usually in a single step),[13,14] and their ability to respond versus physical or chemical stimuli (such as temperature, pressure, or gases),[15−19] allow the introduction of new demand for widely applied optical, electrical, and mechanical materials on the market. Their behavior as semiconductor materials,[20,21] the new recently emerged perspectives related to their easy nanoprocessing[22] (due to their high insolubility in the reaction medium),[23] and the inclusion of structural defects have resulted in increasing interest of these type of compounds in diverse areas such as nanotechnology,[24,25] as smart composite materials with applications as sensors,[26−29] and as novel materials for solar cell technologies.[13]

All of these reasons make them excellent candidates for the manufacture of new composite materials with applications as downshifters in solar cells. The high absorption capacity to UV radiation can be essential to increase the efficient potential of the solar cells in that spectral region, improving the lifetime of photovoltaic cells, and prevents undesirable degradation of some of its components by photoinduced oxidation due to UV radiation.[30]

Received: November 11, 2020
Published: December 30, 2020

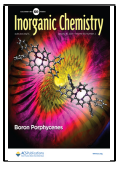

https://dx.doi.org/10.1021/acs.inorgchem.0c03347
Inorg. Chem. 2021, 60, 1208−1219

If we focus only on Cu(I)−I coordination polymers that crystallize as double chains, with the general formula $[Cu(L)I]_n$ (L = pyrimidine, pyrazine organic ligands), the examples found in the literature teach us that slight modifications of the organic ligands allow a wide range of optical properties with compounds that emit in red to compounds that emit in blue.[4,31] The research also shows that these types of coordination polymers have very flexible chains. For this reason, increases or decreases in temperature or pressure,[32] and even the presence of certain types of gases (that can produce supramolecular interactions through hydrogen bonds), slightly modify their structures, causing dramatic changes in their optical and electrical responses.[21] However, this long-studied family of CPs continues to hide significant uncertainties about their behavior in the face of external stimuli and how they are applied. Studies on the variation of emission versus pressure are still limited and are generally with low applied pressures. Indeed, the pressure exerted can be induced in different ways; the material can be ground, subjected to hydrostatic pressure within a diamond cell, or pressed. The effects observed in the emission can be very different depending on the form of pressure exerted. If the pressure exerted is done by grinding, most of the structures published to data suffer amorphization phenomena,[33] which diffuses the study that would allow us to understand the mechanism. In addition, when the material is subjected to compression pressure (pellet manufacturing), phase changes often occur.[25] Finally, studies under hydrostatic pressure are not usually performed because they require techniques beyond most researchers' reach. Recent research has shown that their structures are fascinating since they are incredibly flexible, behaving like a spring under external stimuli.[25] They are founding new behaviors versus gridding or high-pressure experiments that help researchers understand their optical or electrical properties, which can be related to the generation of defects (grinding) or by intermolecular or bond distance modifications.[22]

This work aims to obtain two new Cu(I)−I coordination polymers with Cu_2I_2 double chains and 2,4-diaminopyridine.[34] Their optical and electrical properties have been studied. Additionally, their behavior versus external stimuli (pressure and temperature) has been measured and explained according to theoretical calculations. Finally, the most suitable one has been selected to form composite transparent films with ethyl vinil acetate (EVA) as an organic matrix due to its mechanical processability, high transparency, and chemical and thermal resistance.[35] This new composite material can improve solar cell efficiency by transferring photons from the UV to the visible region at a lower cost than the lanthanide-based sensitizers used at present.

EXPERIMENTAL SECTION

Materials and Methods. All reagents and solvents purchased were used without further purification. Copper iodide (I) (CuI, 99%) and 2,4-diaminopyrimidine (dapym, 98%) were purchased from Sigma-Aldrich (CAS: 7681-65-4 and 156-81-0). Potassium iodine (KI, 99%) was purchased from Alfa Aesar (CAS: 7681-11-0). The solvents used in the synthesis, namely, acetonitrile (CH_3CN) and ethanol (EtOH), were purchased from Labkem and Scharlau with HPLC purification grade (CAS: 75-05-8 and 67-56-1). Poly(ethylene vinyl acetate) (EVA) was purchased from Sigma-Aldrich, with 25% vinyl acetate and 400−900 ppm of BHT as an inhibitor. Trichloroethylene (TCE) was purchased from Panreac and is stabilized in EtOH. TCE was used to improve the dissolution of hot EVA. The dispersion of the coordination polymer in the EVA organic matrix was carried out using a sonication tip Hielscher UP400S (power = 400 W, frequency = 24 kHz).

IR spectra were recorded with a PerkinElmer 100 spectrophotometer using a universal ATR sampling accessory from 4000 to 650 cm^{-1}. Elemental analyses were performed with a LECO CHNS-932 elemental analyzer. Powder X-ray diffraction data were collected using a PANalytical X'Pert PRO diffractometer with a $\theta/2\theta$ primary monochromator and an X'Celerator fast detector and a monochromator 1° for Kα1. The samples have been analyzed with scanning of $\theta/2\theta$, from 3° to 60°, with an angular increase of 0.0167 and a time per increment of 100 s. Thermogravimetric analyses (TGA) were carried out on a TA Instruments Q500 thermobalance oven with a Pt sample holder. Experiments were carried out under nitrogen gas with flow rate of 90 mL/min and heating rate of 10 °C/min, in a temperature range from 25 to 1000 °C. Excitation and emission spectra were recorded in solid samples in the spectral range of 300−1000 nm using a Spex Fluorolog II equipped with a 450 W Xe lamp as the excitation source, two 0.22 m monochromators (Spex 1680) for wavelength selection of the excitation and emission light, respectively, and a cryostat equipped with a vacuum pump to the polycrystalline powders from room temperature (RT, 300 K) to liquid nitrogen temperature (LNT, 80 K). The emission is detected with a 950 V photo multiplier tube (PMT) working in photon counting mode. High-pressure luminescence spectra were recorded on a 0.75 m single grating monochromator (Spex 750M). The excitation source is a 375 nm diode laser excitation (BrixX 200 mW pump power), and a cooled photomultiplier (PMT) (Hamamatsu 928b) was used in detection. For high-pressure measurements up to 10 GPa, a single crystal was placed in a miniature DAC (mini-DAC), designed at the University of Paderborn (Germany) and equipped with an inconel gasket with low luminescent II-a type diamonds for optical and infrared measurements. A mixture of 16:3:1 methanol−ethanol−water was used as a pressure-transmitting medium that provided hydrostatic pressures up to 14 GPa. The hydrostatic pressure was calibrated using the ruby R1 line fluorescence technique. Single-crystal X-ray diffraction (XRD) measurements at ambient pressure and different temperatures (296 and 110 K) were conducted using a Bruker Kappa Apex II diffractometer with graphite-monochromated Mo Kα radiation (λ = 0.71073 Å). The measurements were processed with the CrysAlisPro software. The structures of crystals **1** and **2** at 296 and 110 K were determined by a dual-space algorithm using the SHELXT program, and refinement was performed using SHELXL program against F2 by full-matrix least-squares refinement. The cell parameters were determined and refined by a least-squares fit of all reflections. A semiempirical absorption correction (SADABS) was applied. The structures were also solved by direct methods using the SIR92 program and refined by full-matrix least-squares on F2, including all reflections (SHELXL97). For high-pressure measurements, we have used a Bragg Mini diamond anvil cell (DAC) from Almax-EasyLab, with an opening angle of 85° and anvil culets of 500 μm diameter, fitted with a stainless gasket containing a hole of 200 μm diameter and 75 μm depth. A methanol−ethanol mixture (4:1) was used as the pressure-transmitting medium, which remains hydrostatic in the range of pressure used in our experiments,[36,37] to minimize deviatoric stresses, which can cause incorrect values for bulk modulus.[38] The sample was placed on one of the diamond anvils (diffracted side) together with a small ruby sphere as a pressure sensor. The structure was refined, for each pressure, using previous results as the starting point, on F2 by full-matrix least-squares refinement using the SHELXL program. Due to limitations of the opening angle of our DAC, it is only possible to collect about 20% of the total reflections present in a full data set at ambient conditions. In this situation, structure refinements were performed with isotropic displacement parameters for all atoms except for the heavy atoms (Cu and I) that were refined with anisotropic displacement parameters whenever they did not become nonpositive definite. Hydrogen atoms were included in the final procedure in the same way as for ambient conditions. No restraints were used during this process. Crystallographic data for the structures reported in this contribution have been deposited with the

https://dx.doi.org/10.1021/acs.inorgchem.0c03347
Inorg. Chem. 2021, 60, 1208−1219

Cambridge Crystallographic Data Centre as supplementary publication 2026592−2026608. Copies of the data can be obtained free of charge on application to the CCDC, Cambridge, U.K. (http://www.ccdc.cam.ac.uk/). Scanning electron microscopy (SEM) images were taken in a Philips XL 30 S-FEG electron microscope, applying an electron beam of 300 μA intensity and 10.0 kV potential, at a pressure of 10−7 Pa. To obtain reproducible results, very flat substrates were used with precisely controlled chemical functionalities, freshly prepared just before the samples' chemical deposition. Doped SiO_2 surfaces were sonicated in an ultrasound bath (Elma, 37 kHz, 380 W) for 15 min in acetone and 15 min in 2-propanol and were then dried under an argon flow. After sample preparation, the surfaces were metalized with a 10 nm thick Cr layer, at a pressure of 10−3 Pa. For electrical conductivity measurements, two probe direct current (dc) electrical conductivity measurements at 300 K were performed in four single crystals of compounds **1** and **2**. The conductivity values at 300 K were obtained by applying voltages from −10.0 to +10.0 V. We have performed dc conductivity measurements for at least three single crystals as well as a pressed pellet (at 6.0 GPa, 2 min) of each compound, and the final conductivity value is given by the average value. The contacts were made with Pt wires (25 μm diameter) using graphite paste. The samples were measured in Quantum Design PPMS-9 equipment connected to an external voltage source (Keithley model 2400 source meter) and amperometer (Keithley model 6514 electro-meter). Total reflection X-ray fluorescence (TXRF) analysis was performed using a TXRF 8030C spectrometer (Cameca, France), equipped with a 3 kW X-ray tube with a Mo/W alloy anode with a double-W/C multilayer monochromator adjusted to obtain an excitation energy of 17.4 keV (Mo−Kα) for Cu and I evaluation and a Si(Li) detector with an active area of 80 mm^2 with a resolution of 150 eV at 5.9 keV (Oxford Instruments, England). The measurements were performed working at 50 kV, and the intensity was adjusted automatically so that a count rate of about 8500 cps was achieved. A fixed acquisition time of 500 s was used. External quantum efficiency (EQE) measurements were performed in a setup where the downshifter is placed on a photovoltaic (PV) mini-module based on a single p-type mc-Si solar cell (nontextured and with a SiNx antireflection coating optimized at 600 nm) encapsulated in standard solar glass and showing a 16% conversion efficiency. This solar cell was selected because it shows almost no intrinsic EQE response in the UV spectral region where the downshifting properties of the samples are observed, thus obtaining a direct measure of the increase in EQE produced by the location of the downshifter on the PV mini-module. The EQE setup is based on a standard configuration composed of a 100 W Xe arc lamp, a monochromator, and a digital lock-in amplifier. The PV mini-module is fixed in the EQE set up to ensure the reproducibility of results between samples. Moreover, the glass substrates with EVA and with or without the downshifter are fixed on top of the mini-module in a defined area to ensure the measurements' reproducibility. This configuration produces a loss of efficiency in the 400−1200 nm region for the EQE measurement, placing the PV mini-module and the active species on top compared to the EQE of the bare PV mini-module. It is because there is an air gap between the glass with the active species and the PV mini-module which introduces this loss. An alternative option to avoid this loss is to encapsulate the glass with the active species. Still, we have selected the air gap option because it eases the EQE characterization and comparison with different active species. They are placed in the same area of the PV mini-module and, consequently, guarantee the results' comparison reproducibility.[39] For theoretical calculations, a battery of DFT and TDDFT calculations have been carried out to investigate the electronic and optical properties of the compounds **1** (LT and RT) and **2** (LT) on the basis of the experimental structures and lattices obtained by PXRD. The plane-wave QUANTUM ESPRESSO atomistic simulation code[40] was employed in the calculations. One-electron wave functions are expanded on the basis of plane waves with an energy cutoff of 500 eV for kinetic energy. Electronic exchange and correlation (XC) effects have been accounted for by the revised generalized gradient corrected approximation of Perdew, Burke and Ernzerhof (GGA-PBE).[41] Rappe−Rabe−Kaxiras−Joannopoulos (RRKJ) ultrasoft pseudopotentials have been used to model the ion−electron interaction within the involved atomic species.[42] Brillouin zones (BZ) have been sampled using optimal Monkhorst−Pack grids.[43] We have considered the DFT+D3[44] perturbative correction accounting for the effect of van der Waals (vdW) forces. An empirical vdW correction is added to conventional energy density functionals in order to account for the R-6 behavior of the dispersive forces between atoms. The Fermi level was smeared out using the Methfessel−Paxton approach[45] with a Gaussian width of 0.01 eV, and all energies were extrapolated to T = 0 K. Self-consistency in the electron density was converged to achieve precision in the total energy better than 10−6 eV. The result of these calculations for both compounds reveals a maximum net force acting on any atom below 0.04 eV $Å^{-1}$.

The TDDFT formalism has been employed to compute the excitations and the photoabsorption spectra as implemented in the QUANTUM ESPRESSO simulation package.[46,47] Within this theoretical framework, the excitation spectrum is obtained as $I(\omega) \propto \mathrm{Im}\,[\bar{\alpha}(\omega)]$, where $I(\omega)$ is the absorption intensity, and $\mathrm{Im}[\bar{\alpha}(\omega)]$ is the imaginary part of $\bar{\alpha}$, the averaged (average of the diagonal elements) dipole polarizability. This dynamical polarizability is represented in terms of the resolvent of its Liouvillian superoperator within TDDFT and evaluated using a non-Hermitean Lanczos method, whose implementation does not require the calculation of virtual states.[46,47]

Synthetic Procedures. *Synthesis of 1D-[CuI(dapym)]$_n$ (**1**).* CuI (190 mg, 1.00 mmol) was added with stirring over a saturated solution of KI in H_2O (50 mL) at 25 °C. Over this solution, 2,4-diaminopyrimidine (dapym) (110 mg, 1.00 mmol) was added. The mixture is maintained under magnetic stirring (1600 rpm) for 15 min. White block-shaped crystals of **1**, suitable for X-ray crystallographic analysis, were obtained from the mother solution after 48 h of evaporation at room temperature. The crystals were filtered off, washed with water, and dried in air. Yield: 266 mg (89% based on Cu). Elemental analysis calcd (%) for $C_4H_6CuIN_4$: C 15.98, H 2.02, N 18.64; found C 15.85, H 2.10, N 18.68. IR selected data (ATR): $\tilde{\nu}$ (cm^{-1}): 3471 (vw), 3423 (w), 3353 (m), 3331 (w), 3136 (vw), 1650 (s), 1595 (vs), 1547 (vs), 1504 (m), 1447 (vs), 1384 (s), 1325 (w), 1257 (m), 1122 (w), 1047 (w), 1012 (vw), 794 (w), 781 (w), 675 (w) (Figure S14). The DRX powder diffraction spectrum from the powder shows the same crystal structure that the single crystals have (Figure S7).

*Synthesis of 2D-[Cu$_2$I$_2$(dapym)]$_n$ (**2**).* CuI (381 mg, 2.00 mmol) was added over a saturated KI solution in H_2O (50 mL) at 25 °C. Over this solution, 2,4-diaminopyrimidine (dapym) (110 mg, 1.00 mmol) was added. The mixture is maintained under magnetic stirring (1600 rpm) for 15 min. The solid obtained was filtered off, washed with acetonitrile (2 × 3 mL) and water (2 × 10 mL), and dried in vacuum.

White needle-shaped crystals of **2**, suitable for X-ray crystallographic analysis, were obtained by slow diffusion of diethyl−ether vapor into the mother solution at room temperature after 48 h. Yield: 396 mg (81% based on Cu). Elemental analysis calcd (%) for $C_4H_6Cu_2I_2N_4$: C 9.78, H 1.23, N 11.41; found C 9.25, H 1.38, N 11.00. IR selected data (ATR) $\tilde{\nu}$ (cm^{-1}): 3435 (w), 3392 (m), 3322 (w), 3294 (m), 3195 (vw), 1610 (vs), 1549 (vs), 1486 (m), 1449 (vs), 1387 (s), 1314 (m), 1261 (s), 1044 (vw), 1008 (vw), 793 (vw), 775 (vw), 783 (vw) (Figure S14). The DRX powder diffraction spectrum from the powder shows the same crystal structure that found for the single crystals (Figure S10).

*Synthesis of Composite Material **1@EVA-5%**.* Ethyl vinyl acetate (EVA) polymer was doped with **1** in 5 wt %. First, 0.400 g of EVA was dissolved in 5.5 mL of trichloroethylene (TCE) at 85 °C for 30 min under magnetic stirring (1600 rpm). Then, over this solution, 20.0 mg of **1** was added. Both components were mixed and dispersed by a sonication tip for 15 min at 25 °C (65% amplitude).

By drop-casting, 500 μL of the resulting homogeneous dispersion was deposited on the SiO_2 surfaces (20 × 20 × 2 mm) and dried in air for 48 h to remove TCE by low evaporation. This solution amount is enough to obtain films of micrometric thickness that completely cover

https://dx.doi.org/10.1021/acs.inorgchem.0c03347
Inorg. Chem. 2021, 60, 1208−1219

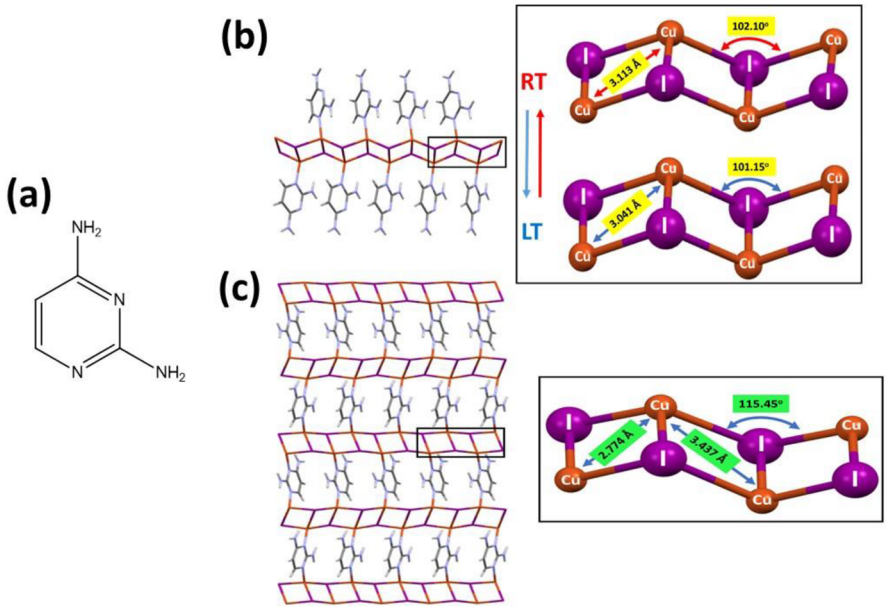

Figure 1. Ligand structure (a) and crystal structures of **1** (b) and **2** (c): View of the crystal structure's packing from the crystallographic *b*-axis (for **1**) and *a*-axis (for **2**). Lateral views of **1** Cu(I)−I double zigzag chains with the Cu−I distances and Cu−I−Cu angles at room temperature (RT, 296 K) and low temperature (LT, 110 K). Cu, orange; I, purple; C, gray; H, white; N, blue.

the glass, which is optimum for the EQE experiments. Finally, the glass is directly placed on a PV mini-module and illuminated for measuring the external quantum efficiency (EQE). The rest of the suspension is deposited in a Petri dish to obtain a film that allows the composite thin film's structural characterization. IR, PXRD, and TXRF analyses showed the presence of **1** in the films (Figures S13, S15, and S35).

RESULTS AND DISCUSSION

Compounds **1** and **2** can be obtained by a direct synthesis between CuI and the 2,4-diaminopyrimidine in acetonitrile and acetonitrile−ethanol at room temperature. These synthetic methods have been described in the Supporting Information (S1.1 and S1.2). However, we have used saturated KI water solutions at room temperature to improve the processes' sustainability, obtaining high reaction yields. The synthesis of **1** was performed at 25 °C, with 1:1 metal−ligand stoichiometry, using a KI saturated water solution to dissolve the CuI adequately. **2** has been obtained with 1:2 metal−ligand stoichiometry, using a similar procedure (KI saturated water solution at 25 °C). The high insolubility in the reaction medium of these coordination polymers allows us to obtain them by fast precipitation. Suitable crystals for single-crystal X-ray diffraction are obtained by diffusion vapors (**2**) or slow evaporation of the mother liquors (**1**).

The IR spectra of the solids obtained (Figures S14 and S15) show the characteristic 2,4-diaminopyrimidine bands displaced by the metal center's coordination to the N1 and/or N3 nitrogen atom positions of the aromatic ring. In addition, thermogravimetric analysis (TGA) was carried out on both compounds. Mass losses, temperature ranges, and interpretations are found in the Experimental Section (Figures S16−S18, Table S4).

The X-ray structures confirm the formation of one-dimensional (**1**) and two-dimensional (**2**) Cu_2I_2 double chains $[Cu(L)I]_n$ (L = 2,4-diaminopyrimidine) (Figure 1), where each Cu(I) atom is coordinated to three iodine atoms and through the ligand by the pyrimidine nitrogen, forming a tetragonal geometry (Figures S1−S4). The iodine atom is three-coordinated, and the pyrimidine ligands preserve their planarity (Figures 1, S1, and S2). Single-crystal data and structure refinement details for compounds **1D-[CuI(dapym)]$_n$** (**1**) and **2D-[Cu_2I_2(dapym)]$_n$** (**2**) at room (RT) and low temperature (LT) are in Table S1.

These double Cu(I)−I chains are a standard coordination mode for this type of coordination polymer.[48,49] Their geometric parameters coincide with the values found in the CSD database for similar copper(I)−iodine stair-cases.[50] The Cu−N distances (2.020 and 2.043 Å) are in the expected ranges for this type of bond (Table S2).[48,51]

The short Cu···Cu distances (3.113 Å for **1** and 2.774 and 3.437 Å for **2**) close to the sum of van der Waals radii of two copper atoms (estimated to be 2.8 Å)[3] are generally the cause of their optoelectronic properties, being semiconductor[20] and luminescent compounds in most cases (Table S2).[52] We have found that **1** and **2** show electrical conductivity values of 10^{-7} and 10^{-8} S cm^{-1}, respectively, at room temperature. These values are in the typical ranges of most conductive coordination polymers (Figures S22−S24). The computed density of electronic states (DOS) as a function of the energy (in eV), referenced to the Fermi level, allow us to obtain theoretical transport gaps between the valence and conduction bands, i.e., 1.90, 1.88, and 1.72 eV for the compounds **1**(LT), **1**(RT), and **2**(LT), respectively (Figure 2).

It is interesting to notice that none of the compounds exhibit an evident n-type or p-type wide-gap semiconducting character, with the Fermi energy located around the midgap region in all cases (Figure 2). As one could expect, **1**(LT) and **1**(RT) show a very similar DOS profile, and the slight structural differences only have a reflection in the tiny reduction of the gap of around 0.02 eV. Nonetheless, the 2D nature of compound **2**(LT) manifests in closing in the bandgap to compound **1**(LT) of 0.18 eV.

Luminescence Properties. As it is known, the emission spectra in CuX-ligand (X = halogen) complexes can be

https://dx.doi.org/10.1021/acs.inorgchem.0c03347
Inorg. Chem. 2021, 60, 1208−1219

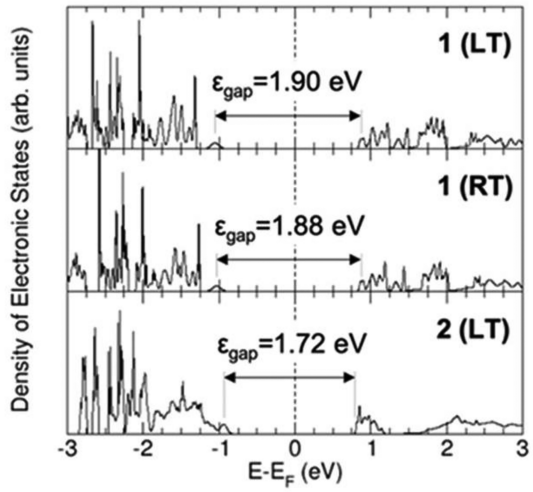

Figure 2. Computed density of electronic states (in arb. units) as a function of the energy (in eV), referenced to the Fermi level, for the compounds **1**(LT), **1**(RT), and **2**(LT). The transport gap, ε_{gap}, between the valence and conduction bands is indicated for all cases.

described in terms of nonexclusive contributions of charge-transfer states as metal-to-ligand MLCT, ligand-to-metal LMCT, halide-to-ligand XLCT, ligand-to-ligand LLCT, ligand-centered LC, and by, as special case, cluster-centered CC, where the transition is localized on the CuI cluster is a combination of halide-to-metal XMCT and metal (copper)-cluster-centered MCC d → s,p character being independent of the ligand. The MCC is related to attraction interactions between the closed d-subshell d^{10} of the Cu atoms in the cluster and requires Cu···Cu distances around, or not much longer than, 2.8 Å (van der Waals radii of two copper atoms) to be important.[9,53−57]

Although both coordination polymers contain the same ligand, their luminescent properties are not similar. These behaviors could be attributed to the different structures they adopt. Given our temperature and pressure results, different emission mechanisms were proposed.

Effect of Hydrostatic Pressure in the Luminescent Behavior of 1 and 2 Poly Crystals. The effect of high pressure (HP) on crystals immersed in hydrostatic conditions also gives us information about the variation of bond distances, volume, and unit-cell parameters. The study was carried out only with a single crystal of **1** (Figures S25−S30) since the single crystal of compound **2** was not stable enough. In the case of **1**, the volume of the tetrahedron formed by Cu as the central atom and the nitrogen and iodine atoms (N1, I1 $I1^{ii}$, and $I1^{iii}$) is affected as is observed in Figures S28 and S29, reducing the value around 15%. We cannot observe indications about phase transition in the range of 2.0 to 7.0 GPa (Figures S25 and S26). The main changes come from an important deformation of the Cu−I ladders sliding from one side to the other and a substantial reorientation of the pyrimidine rings (Figure S27). Thus, the perpendicular distances between pyrimidine rings and their respective slippage distance are also affected (Figure S27). Table S7 shows the volume V, cell parameters (a, b, and c) at equilibrium (displayed as V_0 and L_0), along with the linear moduli M_0 of each axis, the bulk modulus K_0 (both in GPa), and the bulk modules first derivative K'_0. The bulk modulus obtained for **1** falls into the range of 10−20 GPa, which is in the typical range for organometallic compounds[58,59] and similar to other Cu−I ladder compounds.[22,60]

Emission spectra at room temperature (RT) with 375 nm excitation under HP conditions have been recorded up to 11.2 and 10.0 GPa for samples **1** and **2**, respectively, and are shown in Figures 3a and 3b, respectively. In **1**, the behavior of the emission spectra compressing the sample shows different tendencies. At ambient conditions, it consists of a broad symmetric band centered around 590 nm (16950 cm^{-1}) and a full-width at half-maximum (fwhm) of 188 nm (5488 cm^{-1}). This band is dramatically shifted to shorter wavelengths (blue-shift, hypsochromic shift) up to 0.58 GPa with a linear coefficient of 77.6 nm/GPa (−2212 cm^{-1}/GPa). The shift slows at 1.7 GPa, and after this pressure, the trend is reversed and a red-shift (bathochromic shift) with a slower rate of 3.9 nm/GPa (−129 cm^{-1}/GPa) from around 3.0 to 11.0 GPa is observed. An additional band appears at 6.5 GPa at shorter wavelengths with the peak at 450 nm (22220 cm^{-1}), which also red-shifted to compress the sample, with a coefficient rate of 7.8 nm/GPa (−360 cm^{-1}/GPa). In this sample, it is convenient to observe that from ambient conditions to 6.5 GPa some kind of structure is observed between 400 and 450 nm, overlapped with the emission bands; these additional features observed correspond to fluorescence from the II-A

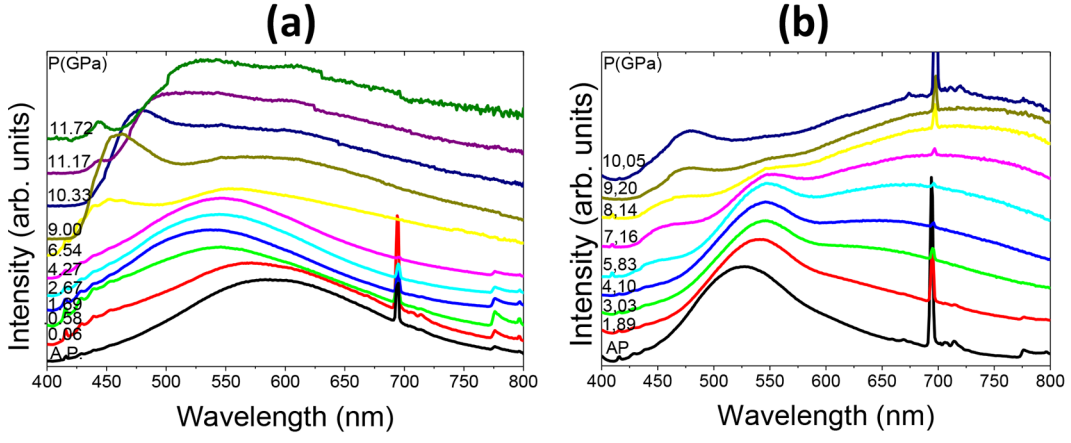

Figure 3. Normalized luminescence spectra of **1** (a) and **2** (b) obtained at 300 K under 375 nm laser excitation for different externally applied hydrostatic pressures, both with a range between 400 and 800 nm. The band at 700 nm corresponds to the ruby emission.

https://dx.doi.org/10.1021/acs.inorgchem.0c03347
Inorg. Chem. 2021, 60, 1208−1219

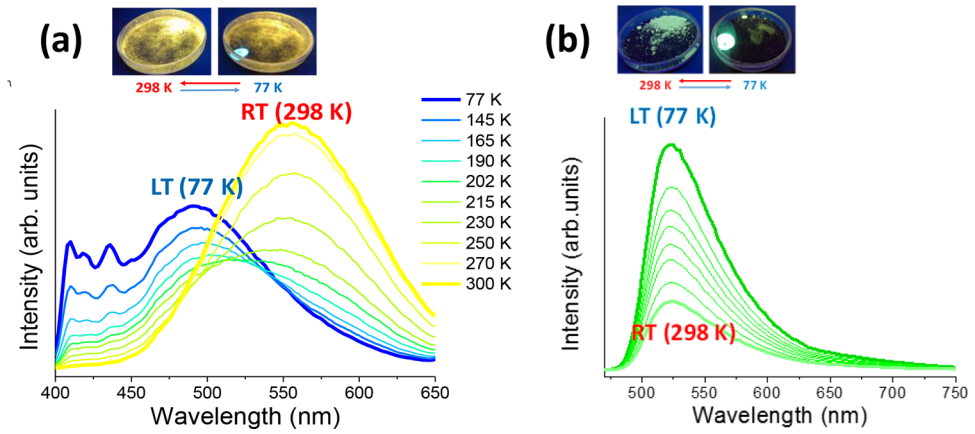

Figure 4. Temperature dependence of photoluminescence emission in solid-state samples for **1** (a) and **2** (b). Visual images of the changes in the emission of compounds **1** and **2** from 298 to 77 K. In both cases, the changes are reversible (top).

type diamond, used in the DAC under UV excitation, which cannot be avoided in the experiment.

Regarding **2**, different results have been found with respect to **1**. At ambient conditions, a symmetric band centered in 525 nm (19048 cm^{-1}) is observed and a full-width at half-maximum (fwhm) of 108 nm (3826 cm-1) is observed, which is narrower than that found in **1**. Up to three different contributions are observed throughout the pressure experiment. The band observed at ambient conditions is progressively shifted to the red with an average of 1.7 nm GPa (−56 cm^{-1}/GPa) from 1.9 to 9.2 GPa. Additionally, at 1.9 GPa, another band overlapped to the previous one emerges at longer wavelengths, and it is more evident at 3.0 GPa, with the maximum peak around 632 nm; this peak is red-shifted, compressing the sample with a rate of 14.7 nm/GPa (−310 cm^{-1}/GPa) up to 10 GPa. On the other hand, and as in **1**, at 6.0 GPa a third band around 445 nm (22470 cm^{-1}) also appears with a red-shift as a function of pressure of 7.5 nm/GPa (−349 cm^{-1}/GPa) up to 10 GPa, which resembles that found in **1**.

Emission of sample **1** along the pressure experiment shows a complex behavior, indicating different mechanisms involved. From AP to 1.4 GPa, a large hypsochromic shift was observed, contrary to the tendency expected for MCC transitions; on the other hand, this is consistent with the fact that in this pressure interval, the Cu−Cu distances are larger than the van der Waals radii, excluding that contribution. However, this behavior is compatible with that known as the rigidochromic effect[61,15] that consists of a hypsochromic shift of the emission band ascribed to ^{3}MLCT states and is a consequence of the increase of the rigidity of the environment when the sample is compressed, as was also observed at a lesser extent in the temperature experiment. On the other hand, the change of tendency of the emission band at 2.7 GPa, where the blue-shift stopped and a bathochromic shift started and became more evident for pressures above 4.3 GPa and beyond, reveals the contributions of other mechanisms involved in the emission. On the basis of the structural information (Figure S26), it can be deduced that at 4.0 GPa the Cu···Cu^{i} distances approach the van der Waals limit for the Cu ions. At this point, the contribution of the ^{3}MCC mechanism became non-negligible and is more relevant as pressure is increased, where the shortening of the Cu···Cu^{i} distances become more evident, around 14% at 9 GPa (2.68 Å) with respect to its value at ambient conditions. Therefore, the competition between the ^{3}MLCT, ^{3}XLCT, and ^{3}MCC emitter states in the pressure interval was measured to explain what is going on in the pressure experiment. On the other hand, the band's intensity increases with pressure up to 3.0 GPa and then rapidly quenches.

Additionally, at around 6.5 GPa, other band peaks at 450 nm show up, overlapping the previous one. The previous band is red-shifted, compressing the sample but with a different rate as compared to the other one. This HE band is usually ascribed to XLCT (ILCT). In our case, it is activated not only at ambient pressure and low temperature but also at ambient temperature and pressures above 6.5 GPa (Figure 3a).

Regarding **2**, the band observed at ambient conditions is narrower and blue-shifted with respect to **1** and shows a different pressure behavior. To explain these differences, we note that, contrary to **1**, there are two different Cu···Cu distances, denoted as Cu−Cu^{ii} and Cu−Cu^{iii} (Table S2), where one falls into the van der Waals limit of 2.8 Å, considering the only data available at LT is for a distance of 2.774 Å and the other is larger (3.457 Å). This fact, together with red-shift with pressure, would indicate that the contribution of the ^{3}MCC transition to the emission of the Cu−Cu^{ii} pairs could be important. The other contribution to the emission at longer wavelengths can be concerned with a shortening of the Cu−Cu^{iii} pairs with pressure. On the other hand, and in the same way that occurs in **1**, a HE band emerges at 6 GPa with a similar pressure behavior as in the previous case, which is also related to the XLCT (ILCT) transition.

The wide band around 525 nm observed at 300 K and 0 GPa for compound **2** moves to longer wavelengths, up to 550 nm, with increasing pressure up to 4.1 GPa (Figure 3b). At 5.8 GPa a new high-energy component appears (440 nm) and joins with the low-energy (LE) component at 550 nm. The low-energy component travels up to 450 nm and increases in intensity, while the high-energy component decreases as the pressure continues to rise to the maximum reached at 10.8 GPa.

Effect of Temperature in the Luminescent Behavior of 1 and 2 Poly Crystals. As we have already mentioned, Cu(I)−I-CPs have attracted recent attention due to their bright luminescence emission and due to their potential applications as smart materials since their emission can vary in response to changes in temperature or pressure.[4,62,63] Their emission energies are strongly affected by the structural changes induced by the heterocyclic organic ligands linked to

https://dx.doi.org/10.1021/acs.inorgchem.0c03347
Inorg. Chem. 2021, 60, 1208−1219

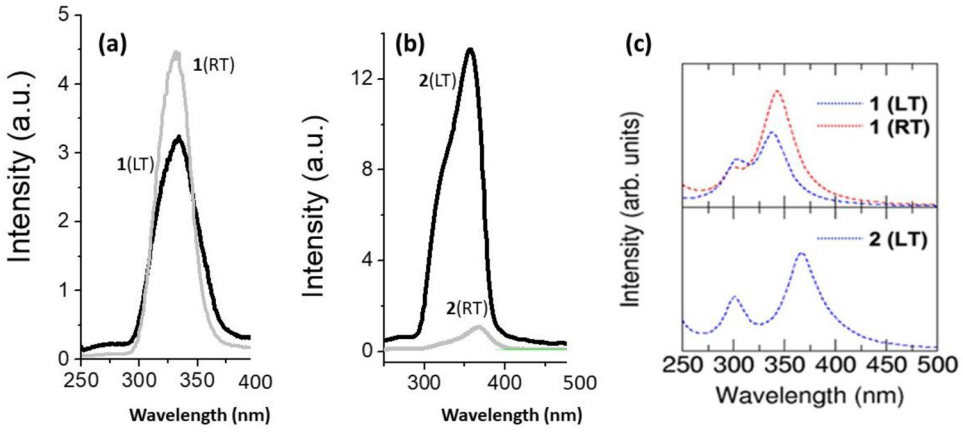

Figure 5. (a) Excitation (λ_{emi} = 490 and 555 nm) spectrum in the solid state of **1** at RT = 298 K (gray line) and LT = 77 K (black line). (b) Excitation (λ_{emi} = 525 nm) spectrum in the solid state of **2** at 298 K (gray green) and 77 K (black line). (c) Computed photoexcitation spectra as a function of the photon wavelength (in nm) for the compounds **1**(LT), **1**(RT), and **2**(LT). Spectra for **1**(LT) and **1**(RT) are shown in the same panel for a better comparison of their photoexcitation intensities.

the metal center of the $[Cu_nI_n]$ chains, by their supramolecular interactions,[10,64,65] or by the variation in Cu−Cu and Cu−X (X = halogen) distances, as well as by variation in their bonding angles. For these reasons, we decided to do a comparative study between coordination polymers **1** and **2**, with Cu_2I_2 chains bridged by the pyrimidine N-heteroaromatic ligand containing in the positions 2 and 4 of the ring, with two amino groups, through solid-state luminescence behavior with similar published compounds, and with similar emission values with similar ligands (Table S5).

To investigate the fluorescence thermochromism properties of the title compounds, emission spectra (excitation 330 nm) at variable temperature (298 to 77 K) were recorded (Figure 4a, b). In the case of **1**, a progressive decrease in the emission intensity and a hypsochromic shift (blue-shift) were observed. The intense emission observed at 555 nm at 298 K is progressively shifted to 492 nm at 77 K (Δ = 63 nm) (Figure 4a). Coordination polymer **2** shows a weak emission band at 525 nm at RT, which progressively increases in intensity by lowering the temperature (Figure 4b). Both compounds exhibited broad emission bands without vibrational progressions since the filled shell d^{10} system for Cu(I) excludes the possibility of d-d transitions.

As we have already mentioned, sample **1** exhibits a 1D chain with symmetrical Cu_2I_2 rhombic core and Cu···Cu distances higher than the sum of the van der Waals radius. At 298 K, the emission is characterized by a broad symmetric band, and the fact of the Cu···Cu distances (see Table S2) commented above excludes the MCC possibility for the emitter state. In addition, the blue-shift observed cooling the sample is compatible with a ^{3}MLCT since it is expected that the temperature induced an increase of the rigidity of the complex.[15,6166] On the other hand, and at intermediate temperatures, the band's shape in terms of its asymmetry suggests more than a unique state involved in the emission. The high-energy component of the band in this kind of complex is usually ascribed to XLCT, so the general emission of **1** can be explained in terms of ^{3}MLCT/^{3}XLCT states in competition.[4,15,67−69]

Additionally, to evaluate the possible presence of emission arising from a ligand-centered (LC) transition, the free ligand 2,4-diaminopyrimidine was also investigated at 298 and 77 K (Figure S19), showing a broad band at 420 nm (λ_{ex} = 330 nm) which increases in intensity when the temperature decreases. This emission corresponds to ligand-centered $\pi \rightarrow \pi^*$ transitions.

However, in **2**, things are quite different since it adopts a 2D double-stranded stair structure with asymmetrical Cu_2I_2 rhombic core where some of the Cu···Cu distances are less than 2.8 Å (see Table S2). This fact may indicate the participation of cluster-centered CC (^{3}XMCT /^{3}MCC) in the emission process. This latter assumption is supported by the differences of the emission band respect to **1**, in its width in its temperature behavior with slight shifts.

The intensity evolution with temperature in this type of compound shows an increase in the emission when the temperature decreases due to the flexibility of the double Cu(I)−I chains, given that the Cu−I and Cu···Cu (Å) distances are shortened. The angles I···Cu···I (deg) are contracted when the temperature decreases due to an increase in their structural rigidity.[70] However, this is not the behavior of compound **1**. To rationalize the origin of the diminishing emission by lowering the temperature, the crystal structure for **1** was measured at 110 K (Figure 1a, Table S1). This experiment allows us to observe that its general structural features do not change with the temperature. Besides this, a slight shortening in the Cu−Cu distances takes place, going from 3.113 Å at 296 K to 3.041 Å at 110 K (Δ = 0.072 Å) (Table S3). The rest of the distances and angles do not suffer from variation (Tables S2 and S3), which is indicative of no significant distortion in the structure upon cooling. Still, trying to explain the slight decrease observed in the emission intensity upon cooling, we have assumed that it could be caused by a change of the organic ligand's molecular configuration, which would confirm the ^{3}MLCT/^{3}XLCT origin. The 2,4-diaminopyrimidine ligands are stacked in a face-to-face fashion with a separation of 4.136 Å at RT between the two organic ligands' centroids, leading to the formation of the 1D chain. Upon cooling, this separation diminishes (4.093 Å at 110 K), indicating an increase in the $\pi-\pi$ stacking between the rings along the chain (Δ = 0.043 Å, Table S3). Such stronger $\pi-\pi$ interactions could modify the energy level of the lowest unoccupied molecular orbital (LUMO).[54] These small changes probably influence the efficiency of the orbital overlapping involved in the electronic transition (see computational details below). We have

https://dx.doi.org/10.1021/acs.inorgchem.0c03347
Inorg. Chem. 2021, 60, 1208−1219

performed theoretical calculations (DOS) for compound **1** (LT) as a proof of concept, forcing the ligands' rotation from the original arrangement to 15°. We have included the graph obtained in the SI (Figure S36). This graph shows a considerable sensitivity of the electron density to the organic ligand rotation. With this experiment, we want to reinforce our theory that small changes in the ligands' orientation caused by pressure or by temperature could induce changes in the LUMO orbital energy.

As is generally expected, **2** exhibits a progressive increase in its emission intensity without shifting of the main band when temperature decreases from 298 to 77 K. This change is probably due to an increase in the structural rigidity, as we have already mentioned. Unfortunately, we could not solve the structure at room temperature due to the single crystals' low quality.

The fact that in both samples nonexponential decay curves were recorded for LE bands (Figures S20 and S21) reinforce the assumption of the contribution to the emission of more than one decay de-excitation mechanism associated with different transitions for these bands.

On the other hand, to establish a direct comparison with the excitation spectra shown in Figure 5a and b, we have computed the photoexcitation spectra as a function of the photon wavelength (in nm) for the compounds **1**(LT), **1**(RT), and **2**(LT). Figure 5c shows the result of these calculations. The figure's top panel shows the spectra for the **1**(LT) and **1**(RT) compounds. Both photoexcitation spectra exhibit a two-peak structure for that wavelength range, with one of the peaks more intense at lower energy and the other one less pronounced at higher energy. The two-peak feature extends in both cases between 275 and 375 nm, with the less intense peaks located at 300 and 290 nm for LT and RT, respectively, and the more pronounced peaks located at 340 and 350 nm, respectively. The more intense excitation peak has its origin in an electronic transition between the valence band (VB), mostly located in the compound's metal skeleton, and the conduction band (CB), mostly located in the ligands (as usual for this kind of compound).[22] At the same time, the less intense peak has its origin in electronic transitions ending in the CB but starting from VB-1 and VB-2 (also located in the metal chain of the compound). A difference in the comparison of these results with the excitation spectra of Figure 5a is noticeable regarding the photon wavelength. Experimentally, the spectra for **1**(LT) and **1**(RT) also show a pronounced feature at similar energy formed by an intense peak and a "shoulder" protrusion at a lower wavelength. The two-peak structure appears resolved by the calculations because no temperature influence can be accounted for in the photoexcitation spectra calculations. Besides this, we can observe a good comparison between both spectra regarding the photoexcitation intensity. Interestingly, compound **1** exhibits a lower signal at LT than at RT, which is an anomalous behavior with respect to a large set of similar compounds, where the behavior is usually the opposite. Although the electronic structure is very similar in both compounds, the slight structural differences from LT to RT may influence the efficiency of the orbital overlapping involved in the electronic transition responsible of the highest peak, since the intensity seems to be the same for the less intense peak at both LT and RT conditions.

On the other side, the bottom panel of Figure 5c shows the photoexcitation spectrum of the **2**(LT) compound. In this case, we also observe a two-peak feature extended between 275 and 425 nm, with the two peaks located at around 300 and 365 nm, again with an excellent agreement with the left panel of Figure 5b. The origin of both peaks is the same as that reported for compounds **1**(LT) and **1**(RT). Interestingly, the photoexcitation threshold for the compound **2** (LT) extends up to a higher wavelength with respect to compound **1**, which is in consistent agreement with a lower band gap value for these compounds.

Moreover, emission lifetimes of the excited state were recorded for **1** and **2** at 298 and 77 K (Figures S20 and S21). As illustrated in Table S6, both coordination polymers fall in the microsecond-order decay, with typical values assigned to phosphorescent emission, arising from a triplet state.[71] Coordination polymer **1** has a higher lifetime than **2**, suggesting a greater rigidity in its structure, probably due to the presence of H-bonds[72] (Figure S4) and, therefore, a higher quantum yield. The nonexponential character of the emission curves' decay curves confirms the participation of more than one state in the emission process in both samples.

Composite Material 1@EVA-5%. The reflectance of **1** in the UV range (Figure S31), its high emission at room temperature, and its nanometric size (Figure S33) make it an excellent candidate to combine with ethyl vinyl acetate (EVA) for the application as a sensibiliser of solar cells. With the idea to maintain a high degree of transparency in the new composite material, and following preliminaries studies, it was decided to use 5% by mass of compound **1** in EVA. The composite material manufacture was done by melting EVA in hot trichloroethylene (TCE), followed by mixing and dispersing **1** in it in a sonication tip.[13] X-ray powder diffraction and IR spectra of composite film **1@EVA-5%** show that the synthesis conditions used for creating hybrid material do not alter the starting material (Figures S13 and S15). Moreover, TXRF measurements indicate a homogeneous distribution of **1** in the film (Figure S35). To confirm that the new composite material retains the starting coordination polymer's intrinsic optical properties, a naked-eye experiment under a UV lamp (λ_{exc} = 254 nm) reveals that **1@EVA-5%** film shows yellow emission at room temperature and blue emission at liquid nitrogen temperature (Figure 6). This process is reversible, and

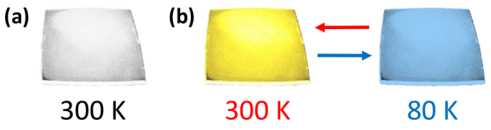

Figure 6. Emission in a naked-eye experiment of **1@EVA-5%** composite film deposited on SiO_2 surfaces under (a) visible light at 300 K and (b) UV light (λ_{exc} = 254 nm) at 300 and 80 K.

thus, warming the materials from 80 to 300 K produces a gradual recovery of their initial emission color. The degree of transparency of the film was measured by UV/visible absorption. As shown in Figure S32, when 5% of **1** is incorporated into EVA, the composite absorbs almost all the incident radiation.

External Quantum Efficiency (EQE) Measurement. The integration of the composite material in the PV mini-module is evaluated by EQE, that is, the amount of current that the cell produces when it is irradiated by photons at a certain wavelength.

As shown in Figure 7, a response has been verified in the UV spectral range when **1@EVA-5%** is incorporated into the Si

https://dx.doi.org/10.1021/acs.inorgchem.0c03347
Inorg. Chem. 2021, 60, 1208−1219

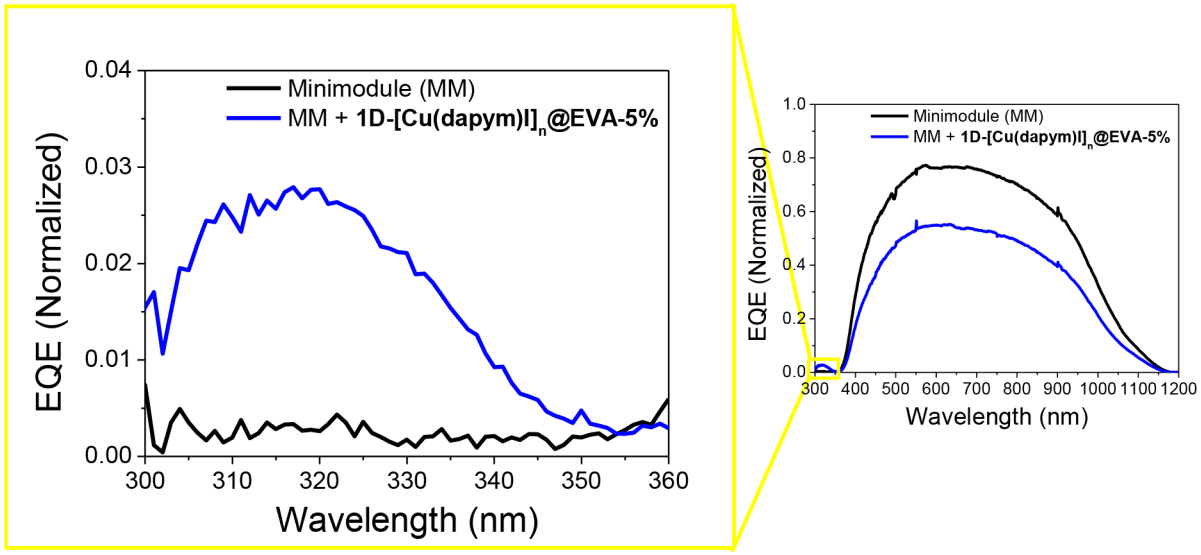

Figure 7. External quantum efficiency (EQE) spectrum collected for **1@EVA-5%** composite film (blue line) deposited in a Si photovoltaic mini-module (black line), in a wavelength range from 300 to 1200 nm at 300 K. Boxed figure: UV zone extension (300−360 nm).

photovoltaic mini-module, with respect to the PV mini-module (MM) covered only with the bare glass, whose EQE value is close to zero. This slight increase in the UV region (300−360 nm) translates into an increase in conversion efficiency in this spectral range. Then, it becomes clear that **1** is an active species with application in solar cells since it is capable of moving the photons of the incident radiation (UV region) to longer wavelengths, where the Si solar cell shows higher conversion efficiency (visible region); this avoids absorption and reflection losses of the photons, as well as parasitic absorptions.[73−75]

CONCLUSIONS

This work demonstrates the interesting optical properties exhibited by the Cu(I)−I coordination polymers based on substituted pyrimidine-derived ligands. In this case, the use of the appropriate ligand, 2,4-diaminopyrimidine (**dapym**), makes it possible to obtain both the one-dimensional and two-dimensional structures by modifying the stoichiometry of the chemical reaction. Although the vast majority of these compounds are obtained in organic solvents (such as acetonitrile) and solvothermal conditions, sustainable water synthesis at room temperature is feasible, obtaining the compounds with a high yield (approximately 90%). Despite presenting the same organic ligand, their structural differences (symmetrical or asymmetrical Cu_2I_2 rhombic cores or change of the organic ligand's molecular configuration) drastically change their emission and response to external stimuli such as temperature. Experimental studies (such as the crystal structure solution at low temperatures or the analysis of crystal structures at different hydrostatic pressures) and theoretical studies (such as the functional theory of density) help us to understand their different properties and their different behaviors.

The UV absorption of compound **1** (around 250 nm), its intense emission in the visible range (555 nm at 330 nm excitation) at room temperature, as well as the ability to be nanoprocessed by instantaneous precipitation in the reaction medium allow us to combine it at 5% by weight with EVA as an organic matrix. The drop-casting deposition method allows us to generate a mechanically flexible composite material with a high degree of transparency and the ability to move the photons of the incident radiation (UV region) to longer wavelengths. Also, the price of copper coordination polymers useful as downshifter solar cells is lower compared with that of the lanthanides complexes.[13] For these reasons, compound **1** can be a right candidate for creating new composite materials with potential applications in solar cell devices.

ASSOCIATED CONTENT

Supporting Information

The Supporting Information is available free of charge at https://pubs.acs.org/doi/10.1021/acs.inorgchem.0c03347.

(S1) Structure characterization, (S2) infrared spectroscopy; (S3) thermogravimetric analysis; (S4) electrical behavior study; (S5) photoluminescent studies; (S6) high-pressure and EoS analysis; (S7) UV−visible spectroscopy; (S8) SEM images; (S9) effect of gridding in the luminescent behavior of **1** and **2** polycrystals; and (S10) TXRF analysis (PDF)

Accession Codes

CCDC 2026592−2026608 contain the supplementary crystallographic data for this paper. These data can be obtained free of charge via www.ccdc.cam.ac.uk/data_request/cif, or by emailing data_request@ccdc.cam.ac.uk, or by contacting The Cambridge Crystallographic Data Centre, 12 Union Road, Cambridge CB2 1EZ, UK; fax: +44 1223 336033.

AUTHOR INFORMATION

Corresponding Author

Pilar Amo-Ochoa − *Facultad de Ciencias, Dpto. Química Inorgánica and Institute for Advanced Research Chemistry (IAdChem), Universidad Autónoma de Madrid, 28049 Madrid, Spain;* orcid.org/0000-0002-1952-1020; Email: pilar.amo@uam.es

Authors

Jesus López − *Facultad de Ciencias, Dpto. Química Inorgánica, Universidad Autónoma de Madrid, 28049 Madrid, Spain*

Javier González Platas − *Departamento de Física, Instituto Universitario de Estudios Avanzados en Física Atómica, Molecular y Fotónica (IUDEA), Universidad de La Laguna, La Laguna, Tenerife E-38204, Spain;* orcid.org/0000-0003-3339-2998

Ulises Ruymán Rodríguez-Mendoza − *Departamento de Física, Instituto Universitario de Estudios Avanzados en Física Atómica, Molecular y Fotónica (IUDEA), Universidad de La Laguna, La Laguna, Tenerife E-38204, Spain;* orcid.org/0000-0002-1431-8488

José Ignacio Martínez − *Departamento de Nanoestructuras, Superficies, Recubrimientos y Astrofísica Molecular, Instituto de Ciencia de Materiales de Madrid (ICMM-CSIC), 28049 Madrid, Spain*

Salomé Delgado − *Facultad de Ciencias, Dpto. Química Inorgánica, Universidad Autónoma de Madrid, 28049 Madrid, Spain*

Ginés Lifante-Pedrola − *Facultad de Ciencias, Dpto. Física de Materiales, Universidad Autónoma de Madrid, 28049 Madrid, Spain*

Eugenio Cantelar − *Facultad de Ciencias, Dpto. Física de Materiales, Universidad Autónoma de Madrid, 28049 Madrid, Spain*

Ricardo Guerrero-Lemus − *Departamento de Física, Universidad de La Laguna, 38207 San Cristóbal de La Laguna, Spain*

Cecilio Hernández-Rodríguez − *Departamento de Física, Universidad de La Laguna, 38207 San Cristóbal de La Laguna, Spain*

Complete contact information is available at: https://pubs.acs.org/10.1021/acs.inorgchem.0c03347

Author Contributions

The manuscript was written through the contributions of all authors. All authors have given approval to the final version of the manuscript.

Notes

The authors declare no competing financial interest.

■ ACKNOWLEDGMENTS

This work has been partially supported by the Ministerio de Ciencia e Innovación (MICIIN) under the National Program of Sciences and Technological Materials (PID2019-106383GB-C44) and the Ministerio de Economía y Competitividad de España (MINECO) under the National Program of Materials (PID2019-108028GB-C22; PID2019-110632RB-100), the National Program Retos (RTI2018-095563-B-I00), and by EU-FEDER funds. J.G.P. thanks Servicios Generales de Apoyo a la Investigación (SEGAI) at Laguna University for support. The authors also thank María Murillo for her help.

■ REFERENCES

(1) Hu, L. X.; Gao, M.; Wen, T.; Kang, Y.; Chen, S. Synthesis of Halide-Modulated Cuprous(I) Coordination Polymers with Mechanochromic and Photocatalytic Properties. *Inorg. Chem.* **2017**, *56*, 6507−6511.

(2) Hartl, H.; Mahdjour-Hassan-Abadi, F. $[(C_6H_5)_4P]\ \infty 1[Cu_3I_4]$—The First Compound with a Helical Chain of Face-Sharing Tetrahedra as a Structural Element. *Angew. Chem., Int. Ed. Engl.* **1994**, *33*, 1841−1842.

(3) Vitale, M.; Ford, P. C. Luminescent mixed ligand copper(I) clusters (CuI)n(L)m (L = pyridine, piperidine): thermodynamic control of molecular and supramolecular species. *Coord. Chem. Rev.* **2001**, *219*−*221*, 3−16.

(4) Araki, H.; Tsuge, K.; Sasaki, Y.; Ishizaka, S.; Kitamura, N. Luminescence Ranging from Red to Blue: A Series of Copper(I)−Halide Complexes Having Rhombic $\{Cu_2(\mu\text{-}X)_2\}$ (X = Br and I) Units with N-Heteroaromatic Ligands. *Inorg. Chem.* **2005**, *44*, 9667−9675.

(5) Armaroli, N.; Accorsi, G.; Cardinali, F.; Listorti, A. Photochemistry and Photophysics of Coordination Compounds:Copper. *Top. Curr. Chem.* **2007**, *280*, 69.

(6) Peng, R.; Li, M.; Li, D. Copper(I) halides: A versatile family in coordination chemistry and crystal engineering. *Coord. Chem. Rev.* **2010**, *254*, 1−18.

(7) Kitada, N.; Ishida, T. Polymeric one- and two-dimensional copper(i) iodide complexes showing photoluminescence tunable by azaaromatic ligands. *CrystEngComm* **2014**, *16*, 8035−8040.

(8) Khatri, N. M.; Pablico-Lansigan, M. H.; Boncher, W. L.; Mertzman, J. E.; Labatete, A. C.; Grande, L. M.; Wunder, D.; Prushan, M. J.; Zhang, W.; Halasyamani, P. S.; Monteiro, J. H.S.K.; Bettencourt-Dias, A. d.; Stoll, S. L. Bettencourt-Dias, A. d.; Stoll, S. L., Luminescence and Nonlinear Optical Properties in Copper(I) Halide Extended Networks. *Inorg. Chem.* **2016**, *55*, 11408−11417.

(9) Troyano, J.; Perles, J.; Amo-Ochoa, P.; Martínez, J. I.; Concepcion Gimeno, M.; Fernandez-Moreira, V.; Zamora, F.; Delgado, S. Luminescent Thermochromism of 2D Coordination Polymers Based on Copper(I) Halides with 4-Hydroxythiophenol. *Chem. - Eur. J.* **2016**, *22*, 18027−18035.

(10) Pospisil, J.; Jess, I.; Näther, C.; Necas, M.; Taborsky, P. Luminescence properties of "double-stranded staircase" copper(i) halide coordination polymers with N-containing ligands. *New J. Chem.* **2011**, *35*, 861−864.

(11) Vitale, M.; Palke, W. E.; Ford, P. C. Origins of the double emission of the tetranuclear copper(I) cluster Cu4I4(pyridine)4: an ab initio study. *J. Phys. Chem.* **1992**, *96*, 8329−8336.

(12) Safko, J. P.; Kuperstock, J. E.; McCullough, S. M.; Noviello, A. M.; Li, X.; Killarney, J. P.; Murphy, C.; Patterson, H. H.; Bayse, C. A.; Pike, R. D. Network formation and photoluminescence in copper(i) halide complexes with substituted piperazine ligands. *Dalton T.* **2012**, *41*, 11663−11674.

(13) López-Molina, J.; Hernández-Rodríguez, C.; Guerrero-Lemus, R.; Cantelar, E.; Lifante, G.; Muñoz, M.; Amo-Ochoa, P. Cu(i)−I coordination polymers as the possible substitutes of lanthanides as downshifters for increasing the conversion efficiency of solar cells. *Dalton Trans.* **2020**, *49*, 4315−4322.

(14) Wang, R.-Y.; Zhang, X.; Yu, J.-H.; Xu, J.-Q. Copper(i)−polymers and their photoluminescence thermochromism properties. *Photoch. Photobio. Sci.* **2019**, *18*, 477−486.

(15) Tran, D.; Bourassa, J. L.; Ford, P. C. Pressure-Induced Luminescence Rigidochromism in the Photophysics of the Cuprous Iodide Cluster Cu4I4py4. *Inorg. Chem.* **1997**, *36*, 439−442.

(16) Jeß, I.; Taborsky, P.; Pospíšil, J.; Näther, C. Synthesis, crystal structure, thermal and luminescence properties of CuX(2,3-dimethylpyrazine) (X = Cl, Br, I) coordination polymers. *Dalton Trans.* **2007**, *22*, 2263−2270.

(17) Kim, T. H.; Shin, Y. W.; Kim, J. S.; Lee, S. S.; Kim, J. Luminescent staircase copper(I) coordination polymer based on planar Cu3I3. *Inorg. Chem. Commun.* **2007**, *10*, 717−719.

(18) Benito, Q.; Le Goff, X. F.; Maron, S.; Fargues, A.; Garcia, A.; Martineau, C.; Taulelle, F.; Kahlal, S.; Gacoin, T.; Boilot, J. P.; Perruchas, S. Polymorphic Copper Iodide Clusters: Insights into the Mechanochromic Luminescence Properties. *J. Am. Chem. Soc.* **2014**, *136*, 11311−11320.

(19) Cariati, E.; Bourassa, J. Luminescence response of the solid state polynuclear copper(I) iodide materials [CuI(4-picoline)] to volatile organic compounds. *Chem. Commun.* **1998**, *16*, 1623−1624.

(20) Givaja, G.; Amo-Ochoa, P.; Gomez-Garcia, C. J.; Zamora, F. Electrical conductive coordination polymers. *Chem. Soc. Rev.* **2012**, *41*, 115−147.

(21) Hassanein, K.; Amo-Ochoa, P.; Gomez-Garcia, C. J.; Delgado, S.; Castillo, O.; Ocon, P.; Martinez, J. I.; Perles, J.; Zamora, F. Halo and Pseudohalo Cu(I)-Pyridinato Double Chains with Tunable Physical Properties. *Inorg. Chem.* **2015**, *54*, 10738−10747.
(22) Conesa-Egea, J.; González-Platas, J.; Rodríguez-Mendoza, U. R.; Martínez, J. I.; Pilar, O.; Fernández-Moreira, V.; Costa, R. D.; Fernández-Cestau, J.; Zamora, F.; Amo-Ochoa, P. Cunning defects: emission control by structural point defects on Cu(i)I double chain coordination polymers. *J. Mater. Chem. C* **2020**, *8*, 1448−1458.
(23) Conesa-Egea, J.; Gallardo-Martinez, J.; Delgado, S.; Martinez, J. I.; Gonzalez-Platas, J.; Fernandez-Moreira, V.; Rodriguez-Mendoza, U. R.; Ocon, P.; Zamora, F.; Amo-Ochoa, P. Multistimuli Response Micro- and Nanolayers of a Coordination Polymer Based on Cu_2I_2 Chains Linked by 2-Aminopyrazine. *Small* **2017**, *13*, 1700965.
(24) Conesa-Egea, J.; Nogal, N.; Martínez, J. I.; Fernández-Moreira, V.; Rodríguez-Mendoza, U. R.; González-Platas, J.; Gómez-García, C. J.; Delgado, S.; Zamora, F.; Amo-Ochoa, P. Smart composite films of nanometric thickness based on copper−iodine coordination polymers. Toward sensors. *Chem. Sci.* **2018**, *9*, 8000−8010.
(25) Conesa-Egea, J.; Zamora, F.; Amo-Ochoa, P. Perspectives of the smart Cu-Iodine coordination polymers: A portage to the world of new nanomaterials and composites. *Coord. Chem. Rev.* **2019**, *381*, 65−78.
(26) Song, Y.; Fan, R.; Wang, P.; Wang, X.; Gao, S.; Du, X.; Yang, Y.; Luan, T. Copper(i)-iodide based coordination polymers: bifunctional properties related to thermochromism and PMMA-doped polymer film materials. *J. Mater. Chem. C* **2015**, *3*, 6249−6259.
(27) Song, Y.; Fan, R. Q.; Zhang, H. J.; Liu, Z. W.; Wang, X. T.; Tan, C. T.; Yang, Y. L.; Wang, Y. L. Luminescent properties of Ag(I)/Cu(I) coordination polymers: crystal structures and high intensity luminescence of a PMMA-doped hybrid material based on a quinoline-2,3-dicarboxylic acid ligand. *RSC Adv.* **2015**, *5*, 17343−17353.
(28) Zhao, C.-W.; Ma, J.-P.; Liu, Q.-K.; Wang, X.-R.; Liu, Y.; Yang, J.; Yang, J.-S.; Dong, Y.-B. An in situ self-assembled Cu_4I_4-MOF-based mixed matrix membrane: a highly sensitive and selective naked-eye sensor for gaseous HCl. *Chem. Commun.* **2016**, *52*, 5238−5241.
(29) Conesa-Egea, J.; Moreno-Vázquez, A.; Fernández-Moreira, V.; Ballesteros, Y.; Castellanos, M.; Zamora, F.; Amo-Ochoa, P. Micro and Nano Smart Composite Films Based on Copper-Iodine Coordination Polymer as Thermochromic Biocompatible Sensors. *Polymers* **2019**, *11*, 1047.
(30) Day, J.; Senthilarasu, S.; Mallick, T. K. Improving spectral modification for applications in solar cells: A review. *Renewable Energy* **2019**, *132*, 186−205.
(31) Thébault, F.; Barnett, S. A.; Blake, A. J.; Wilson, C.; Champness, N. R.; Schröder, M. Control of Copper(I) Iodide Architectures by Ligand Design: Angular versus Linear Bridging Ligands. *Inorg. Chem.* **2006**, *45*, 6179−6187.
(32) Kim, T. H.; Shin, Y. W.; Jung, J. H.; Kim, J. S.; Kim, J. Crystal-to-Crystal Transformation between Three CuI Coordination Polymers and Structural Evidence for Luminescence Thermochromism. *Angew. Chem.* **2008**, *120*, 697−700.
(33) Kobayashi, A.; Yoshida, Y.; Yoshida, M.; Kato, M. Mechanochromic Switching between Delayed Fluorescence and Phosphorescence of Luminescent Coordination Polymers Composed of Dinuclear Copper(I) Iodide Rhombic Cores. *Chem. - Eur. J.* **2018**, *24*, 14750−14759.
(34) Ma, W.-F.; Yang, H.-K.; Hu, M.-J.; Li, Q.; Ma, T.-Z.; Zhou, Z.-Z.; Liu, R.-Y.; You, W.-W.; Zhao, P.-L. One-pot synthesis and antiproliferative activity of novel 2,4-diaminopyrimidine derivatives bearing piperidine and piperazine moieties. *Eur. J. Med. Chem.* **2014**, *84*, 127−134.
(35) Kumi, D.; Khan, S.; Cho, S.-H.; Ntwaeaborwa, O. Ultraviolet to visible down conversion of SiO^{2-} Ce^{3+}, Tb^{3+} nanospheres-poly-EVA films for solar cell application. *Phys. B. Phys. B* **2020**, *576*, 411711.
(36) Scheidl, K. S.; Kurnosov, A.; Trots, D. M.; Boffa Ballaran, T.; Angel, R. J.; Miletich, R. Extending the single-crystal quartz pressure gauge up to hydrostatic pressure of 19 GPa. *J. Appl. Crystallogr.* **2016**, *49*, 2129−2137.
(37) Efthimiopoulos, I.; Ritscher, A.; Lerch, M.; Speziale, S.; Pakhomova, A. S.; Liermann, H. P.; Koch-Müller, M. Structural transitions of ordered kesterite-type Cu2ZnSnS4 under pressure. *Appl. Phys. Lett.* **2017**, *110*, No. 041905.
(38) Errandonea, D.; Muñoz, A.; Gonzalez-Platas, J. Comment on "High-pressure x-ray diffraction study of YBO3/Eu3+, GdBO3, and EuBO3: Pressure-induced amorphization in GdBO3. *J. Appl. Phys.* **2014**, *115*, 216101.
(39) Guerrero-Lemus, R.; Sanchiz, J.; Sierra, M.; Martín, I. R.; Hernández-Rodríguez, C.; Borchert, D. Alternative and fully experimental procedure for characterizing down-shifters placed on photovoltaic devices. *Sol. Energy Mater. Sol. Cells* **2018**, *185*, 312−317.
(40) Giannozzi, P.; Baroni, S.; Bonini, N.; Calandra, M.; Car, R.; Cavazzoni, C.; Ceresoli, D.; Chiarotti, G. L.; Cococcioni, M.; Dabo, I.; Dal Corso, A.; de Gironcoli, S.; Fabris, S.; Fratesi, G.; Gebauer, R.; Gerstmann, U.; Gougoussis, C.; Kokalj, A.; Lazzeri, M.; Martin-Samos, L.; Marzari, N.; Mauri, F.; Mazzarello, R.; Paolini, S.; Pasquarello, A.; Paulatto, L.; Sbraccia, C.; Scandolo, S.; Sclauzero, G.; Seitsonen, A. P.; Smogunov, A.; Umari, P.; Wentzcovitch, R. M. QUANTUM ESPRESSO: a modular and open-source software project for quantum simulations of materials. *J. Phys.: Condens. Matter* **2009**, *21*, 395502.
(41) Slone, R. V.; Hupp, J. T.; Stern, C. L.; Albrecht-Schmitt, T. E. Self-Assembly of Luminescent Molecular Squares Featuring Octahedral Rhenium Corners. *Inorg. Chem.* **1996**, *35*, 4096−4097.
(42) Rappe, A. M.; Rabe, K. M.; Kaxiras, E.; Joannopoulos, J. D. Optimized pseudopotentials. *Phys. Rev. B: Condens. Matter Mater. Phys.* **1990**, *41*, 1227−1230.
(43) Monkhorst, H. J.; Pack, J. D. Special points for Brillouin-zone integrations. *Phys. Rev.B* **1976**, *13*, 5188−5192.
(44) Grimme, S.; Antony, J.; Ehrlich, S.; Krieg, H. A consistent and accurate ab initio parametrization of density functional dispersion correction (DFT-D) for the 94 elements H-Pu. *J. Chem. Phys.* **2010**, *132*, 154104.
(45) Methfessel, M.; Paxton, A. T. High-precision sampling for Brillouin-zone integration in metals. *Phys. Rev. B: Condens. Matter Mater. Phys.* **1989**, *40*, 3616−3621.
(46) Malcioglu, B.; Gebauer, R.; Rocca, D.; Baroni, S. TurboTDDFT - A code for the simulation of molecular spectra using the Liouville-Lanczos approach to time-dependent density-functional perturbation theory. *Comput. Phys. Commun.* **2011**, *182*, 1744−1754.
(47) Ge, X.; Binnie, S. J.; Rocca, D.; Gebauer, R.; Baroni, S. turboTDDFT 2.0—Hybrid functionals and new algorithms within time-dependent density-functional perturbation theory. *Comput. Phys. Commun.* **2014**, *185*, 2080−2089.
(48) Blake, A. J.; Brooks, N. R.; Champness, N. R.; Cooke, P. A.; Crew, M.; Deveson, A. M.; Hanton, L. R.; Hubberstey, P.; Fenske, D.; Schröder, M. Copper(I) iodide coordination networks−controlling the placement of (CuI)∞ ladders and chains within two-dimensional sheets. *Cryst. Eng.* **1999**, *2*, 181−195.
(49) Bosch, E. Coordination Network Formed Between 5,5′-Bipyrimidine and Copper(I) Iodide. *J. Chem. Crystallogr.* **2012**, *42*, 455−457.
(50) Allen, F. The Cambridge Structural Database: a quarter of a million crystal structures and rising. *Acta Crystallogr., Sect. B: Struct. Sci.* **2002**, *58*, 380−388.
(51) Kozlev, B.; Murn, A.; Podlipnik, K.; Lah, N.; Leban, I. Two Types of Pyridine Ligands in Mononuclear and Dinuclear Copper(II) Carboxylates. *Croatica Chemica Acta* **2004**, *77*, 613−618.
(52) Troyano, J.; Castillo, O.; Amo-Ochoa, P.; Fernandez-Moreira, V.; Gomez-Garcia, C. J.; Zamora, F.; Delgado, S. A crystalline and free-standing silver thiocarboxylate thin-film showing high green to yellow luminescence. *J. Mater. Chem. C* **2016**, *4*, 8545−8551.
(53) Liu, W.; Fang, Y.; Wei, G. Z.; Teat, S. J.; Xiong, K.; Hu, Z.; Lustig, W. P.; Li, J. A Family of Highly Efficient CuI-Based Lighting

Phosphors Prepared by a Systematic, Bottom-up Synthetic Approach. *J. Am. Chem. Soc.* **2015**, *137*, 9400−9408.
(54) Manbeck, G. F.; Brennessel, W. W.; Evans, C. M.; Eisenberg, R. Tetranuclear Copper(I) Iodide Complexes of Chelating Bis(1-benzyl-1H-1,2,3-triazole) Ligands: Structural Characterization and Solid State Photoluminescence. *Inorg. Chem.* **2010**, *49*, 2834−2843.
(55) Kyle, K. R.; Ryu, C. K.; Ford, P. C.; DiBenedetto, J. A. Photophysical studies in solution of the tetranuclear copper(I) clusters Cu4I4L4 (L = pyridine or substituted pyridine). *J. Am. Chem. Soc.* **1991**, *113*, 2954−2965.
(56) Vitale, M.; Ryu, C. K.; Palke, W. E.; Ford, P. C. Ab initio studies of the copper(I) tetramers $Cu_4X_4L_4$ (X = I, Br, Cl). Effects of cluster structure and of halide on photophysical properties. *Inorg. Chem.* **1994**, *33*, 561−566.
(57) Ford, P. C.; Cariati, E.; Bourassa, J. Photoluminescence Properties of Multinuclear Copper(I) Compounds. *Chem. Rev.* **1999**, *99*, 3625−3648.
(58) Spencer, E. C.; Angel, R. J.; Ross, N. L.; Hanson, B. E.; Howard, J. A. K. Pressure-Induced Cooperative Bond Rearrangement in a Zinc Imidazolate Framework: A High-Pressure Single-Crystal X-Ray Diffraction Study. *J. Am. Chem. Soc.* **2009**, *131*, 4022−4026.
(59) Funnell, N. P.; Dawson, A.; Francis, D.; Lennie, A. R.; Marshall, W. G.; Moggach, S. A.; Warren, J. E.; Parsons, S. The effect of pressure on the crystal structure of l-alanine. *CrystEngComm* **2010**, *12*, 2573−2583.
(60) Aguirrechu-Comerón, A.; Hernández-Molina, R.; Rodríguez-Hernández, P.; Muñoz, A.; Rodríguez-Mendoza, U. R.; Lavín, V. c.; Angel, R. J.; Gonzalez-Platas, J. Experimental and ab Initio Study of Catena(bis(μ2-iodo)-6-methylquinoline-copper(I)) under Pressure: Synthesis, Crystal Structure, Electronic, and Luminescence Properties. *Inorg. Chem.* **2016**, *55*, 7476−7484.
(61) Lees, A. J. The Luminescence Rigidochromic Effect Exhibited by Organometallic Complexes: Rationale and Applications. *Comments Inorg. Chem.* **1995**, *17*, 319−346.
(62) Zhang, X.; Liu, W.; Wei, G. Z.; Banerjee, D.; Hu, Z.; Li, J. Systematic Approach in Designing Rare-Earth-Free Hybrid Semiconductor Phosphors for General Lighting Applications. *J. Am. Chem. Soc.* **2014**, *136*, 14230−14236.
(63) Mirzaahmadi, A.; Hosseini-Yazdi, S. A.; Safarzadeh, E.; Baradaran, B.; Samolova, E.; Dusek, M. New series of water-soluble thiosemicarbazones and their copper(II) complexes as potentially promising anticancer compounds. *J. Mol. Liq.* **2019**, *293*, 111412.
(64) Li, J.-C.; Li, H.-X.; Li, H.-Y.; Gong, W.-J.; Lang, J.-P. Ligand Coordination Site-Directed Assembly of Copper(I) Iodide Complexes of ((Pyridyl)-1-pyrazolyl)pyridine. *Cryst. Growth Des.* **2016**, *16*, 1617−1625.
(65) Užarević, K.; Štrukil, V.; Mottillo, C.; Julien, P. A.; Puškarić, A.; Friščić, T.; Halasz, I. Exploring the Effect of Temperature on a Mechanochemical Reaction by in Situ Synchrotron Powder X-ray Diffraction. *Cryst. Growth Des.* **2016**, *16*, 2342−2347.
(66) Crane, D. R.; Ford, P. C. Pressure effects on the competitive energy and electron transfer quenching of the MLCT excited state of $Cu(dpp)^{2+}$ (dpp = 2,9-diphenyl-1,10-phenanthroline) by CrL_3 (L = .beta.-dionato ligands) and other quenchers in solution. *J. Am. Chem. Soc.* **1991**, *113*, 8510−8516.
(67) Zink, D. M.; Volz, D.; Baumann, T.; Mydlak, M.; Flügge, H.; Friedrichs, J.; Nieger, M.; Bräse, S. Heteroleptic, Dinuclear Copper(I) Complexes for Application in Organic Light-Emitting Diodes. *Chem. Mater.* **2013**, *25*, 4471−4486.
(68) Cariati, E.; Roberto, D.; Ugo, R.; Ford, P. C.; Galli, S.; Sironi, A. X-ray Structures and Emissive and Second-Order Nonlinear Optical Properties of Two Inorganic−Organic Polymeric Adducts of CuI with 4-Acetylpyridine. The Role of Both "Intrastrand" Charge Transfers and Structural Motifs on the Nonlinear Optical Response of Cu(I) Polymeric Adducts with Pseudoaromatic η1-Nitrogen Donor Ligands. *Chem. Mater.* **2002**, *14*, 5116−5123.
(69) Tard, C.; Perruchas, S.; Maron, S.; Le Goff, X. F.; Guillen, F.; Garcia, A.; Vigneron, J.; Etcheberry, A.; Gacoin, T.; Boilot, J.-P. Thermochromic Luminescence of Sol−Gel Films Based on Copper Iodide Clusters. *Chem. Mater.* **2008**, *20*, 7010−7016.
(70) Hassanein, K.; Conesa-Egea, J.; Delgado, S.; Castillo, O.; Benmansour, S.; Martínez, J. I.; Abellán, G.; Gómez-García, C. J.; Zamora, F.; Amo-Ochoea, P. Electrical Conductivity and Strong Luminescence in Copper Iodide Double Chains with Isonicotinato Derivatives. *Chem. - Eur. J.* **2015**, *21*, 17282−17292.
(71) Albrecht, C. Principles of fluorescence spectroscopy. *Anal. Bioanal. Chem.* **2008**, *390*, 1223−1224.
(72) Dhara, K.; Saha, U. C.; Dan, A.; Sarkar, S.; Manassero, M.; Chattopadhyay, P. A new water−soluble copper(ii) complex as a selective fluorescent sensor for azide ion. *Chem. Commun.* **2010**, *46*, 1754−1756.
(73) González-Pérez, S.; Sanchiz, J.; González-Díaz, B.; Holinski, S.; Borchert, D.; Hernández-Rodríguez, C.; Guerrero-Lemus, R. Luminescent polymeric film containing an Eu(III) complex acting as UV protector and down-converter for Si-based solar cells and modules. *Surf. Coat. Technol.* **2015**, *271*, 106−111.
(74) Fix, T.; Nonat, A.; Imbert, D.; Di Pietro, S.; Mazzanti, M.; Slaoui, A.; Charbonnière, L. J. Enhancement of silicon solar cells by downshifting with Eu and Tb coordination complexes. *Prog. Photovoltaics* **2016**, *24*, 1251−1260.
(75) Zucchi, G.; Murugesan, V.; Tondelier, D.; Aldakov, D.; Jeon, T.; Yang, F.; Thuéry, P.; Ephritikhine, M.; Geffroy, B. Solution, Solid State, and Film Properties of a Structurally Characterized Highly Luminescent Molecular Europium Plastic Material Excitable with Visible Light. *Inorg. Chem.* **2011**, *50*, 4851−4856.

https://dx.doi.org/10.1021/acs.inorgchem.0c03347
Inorg. Chem. 2021, 60, 1208−1219